OPEN

NPG Asia Materials (2016) 8, e324; doi:10.1038/am.2016.162
www.nature.com/am

ORIGINAL ARTICLE

Perpendicular magnetic tunnel junction (p-MTJ) spin-valves designed with a top $Co_2Fe_6B_2$ free layer and a nanoscale-thick tungsten bridging and capping layer

Seung-Eun Lee, Tae-Hun Shim and Jea-Gun Park

Recently, p-MTJ spin-valves with top $Co_2Fe_6B_2$ free layers have been widely studied. They potentially experience crystallinity degradation in the face-centered-cubic (fcc) structure of the MgO tunneling barrier as a result of the diffusion of Ta atoms and a significant amount of Fe atoms from the $Co_2Fe_6B_2$ free and pinned layers. A new design of the p-MTJ spin-valve using a nanoscale-thick W bridging and capping layer demonstrated the absence of significant crystallinity degradation in the fcc structure and showed a limited diffusion of Fe atoms, thus achieving a TMR ratio of ~143% at an *ex-situ* annealing temperature of 400 °C.

NPG Asia Materials (2016) **8,** e324; doi:10.1038/am.2016.162; published online 4 November 2016

INTRODUCTION

Recently, dynamic random access memory cells fabricated with a selective transistor and a capacitor (1T1C) have faced a physical limitation when they are scaled down to dimensions below 20 nm.[1–3] Perpendicular spin-transfer-torque magnetic random access memory cells fabricated with a selective transistor and a bi-stable resistance (1T1R) have been studied intensively as a promising solution to overcome this issue in current dynamic random access memory cells, where a bi-stable resistance is formed with a perpendicular magnetic tunnel junction (p-MTJ) spin-valve.[4–11] CoFeB/MgO-based p-MTJ spin-valves have been widely used for realizing the terra-bit-level integration of perpendicular spin-transfer-torque magnetic random access memory cells. These spin-valves need to achieve a high tunneling magnetoresistance (TMR) ratio (>150%), high thermal stability (Δ; >74) and a high switching current (J_c; $\sim 1\times10^2$ MA cm^{-2}) at the back end of line (BEOL) temperature of 400 °C.[12–14] In particular, the p-MTJ spin-valve structure with a top CoFeB free layer has recently been shown to achieve a high TMR ratio at the BEOL temperature of 400 °C.[13–15] Notably, the TMR ratio decreases rapidly as the BEOL temperature increases, so a TMR ratio of >100% at the BEOL temperature of 400 °C is extremely difficult to achieve.[16–18] In this study, we investigated the effect of nanoscale-thick bridging and capping materials ((Tantalum (Ta) or Tungsten (W)) on the TMR ratio at the BEOL temperature of 400 °C for the p-MTJ spin-valve with a top $Co_2Fe_6B_2$ free layer. A bridging layer ferro-couples the $Co_2Fe_6B_2$ pinned layer with an upper synthetic anti-ferromagnetic (SyAF) layer in the p-MTJ spin-valve, and a capping layer is sputtered on the $Co_2Fe_6B_2$ free layer, as shown in Figure 1a and b.[19–21] In addition, the mechanism by which the bridging and capping materials determine the TMR ratio is analyzed by the static perpendicular magnetic anisotropy (PMA) behavior, the face-center-cubic (fcc) crystallinity of the MgO tunneling barrier and the atomic compositional depth profile of the p-MTJ spin-valves.[22]

MATERIALS AND METHODS

Two different p-MTJ spin-valve structures were fabricated on 12-inch-diameter Si/SiO_2/W/TiN bottom electrodes planarized by chemical mechanical polishing, and the structures were produced by the vertical stacking of layers via a multi-chamber sputtering system under a high vacuum pressure of $<1\times10^{-8}$ torr. First, the P-MTJ spin-valve with a nanoscale-thick Ta bridging and capping layer, called the p-MTJ spin-valve (stack **A**), was vertically fabricated from the Si/SiO_2/W/TiN bottom electrode/Ta buffer layer/Pt seed layer/lower($[Co/Pt]_6$/Co) SyAF layer/Ru bridge layer (0.85 nm)/upper(Co/$[Co/Pt]_4$) SyAF layer/Ta bridge layer (0.4 nm)/$Co_2Fe_6B_2$ (1.05 nm) pinned-layer/MgO (1.05 nm) tunnel barrier/Fe (0.4 nm) insert layer/$Co_2Fe_6B_2$ (1.0 nm) free layer/Ta capping layer (1~3 nm)/Ru top electrode structure, as shown in Figure 1a. Second, the p-MTJ spin-valve with a nanoscale-thick W bridging and capping layer, called the p-MTJ spin-valve (stack **B**), was vertically produced with the Si/SiO_2/W/TiN bottom electrode/Ta buffer layer/Pt seed layer/lower ($[Co/Pt]_6$/Co) SyAF layer/Ru bridge layer (0.85 nm)/upper(Co/$[Co/Pt]_4$) SyAF layer/W bridge layer (0.24 nm)/$Co_2Fe_6B_2$ (1.05 nm) pinned-layer/MgO (1.05 nm) tunnel barrier/Fe (0.4 nm) insert layer/$Co_2Fe_6B_2$ (1.0 nm) free layer/W capping(1.6–4.6 nm) layer/Ta buffer(0.5 nm)/Ru top electrode structure, as shown in Figure 1b. Then, all p-MTJ spin-valves were subject to *ex-situ* annealing at a BEOL temperature of 400 °C. Afterward, we examined the mechanism by which the W bridging and capping layers enhance the TMR ratio by analyzing the

MRAM Center, Department of Electronics and Computer Engineering, Hanyang University, Seoul, Republic of Korea
Correspondence: Professor J-G Park, Department of Electronics and Computer Engineering, Hanyang University, 17 Haengdang-dong, Seongdong-gu, Seoul 133-791, Republic of Korea.
E-mail: parkjgl@hanyang.ac.kr
Received 2 April 2016; revised 3 July 2016; accepted 1 August 2016

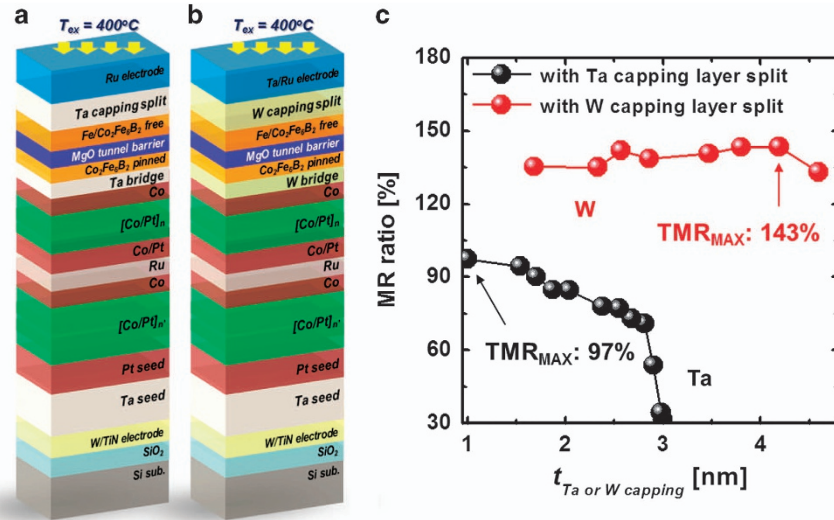

Figure 1 (**a**) p-MTJ spin-valve structure with a Ta bridging and capping layer, (**b**) p-MTJ spin-valve structure with a W bridging and capping layer and (**c**) dependence of the TMR ratio on the bridging and capping layer thickness for both p-MTJ spin-valves with Ta and W bridging and capping layers.

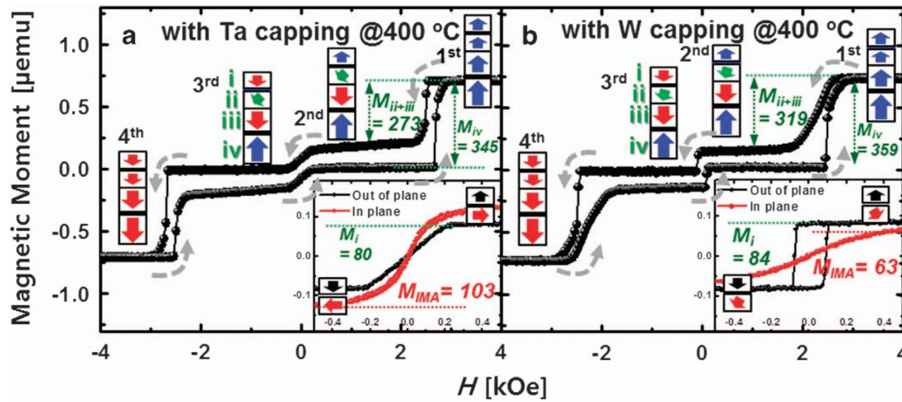

Figure 2 Dependence of static PMA magnetic behavior on bridging and capping materials for the p-MTJ spin-valve. (**a**) *M–H* curve for p-MTJ spin-valve with a Ta bridging and capping layer and (**b**) *M–H* curve for p-MTJ spin-valve with a W bridging and capping layer. The *M–H* curve in the inlet corresponds to the static PMA behavior of a narrow range magnetic field.

following properties of the spin-valves: the TMR ratio by using the current in-plane tunneling at room temperature,[23] the static PMA magnetization behavior by using a 10-inch vibrating sample magnetometer system, the (100) fcc crystallinity of the MgO tunneling barrier with high-resolution transmission electron microscopy (X-HRTEM) at 200 keV, and the atomic-layer compositional depth profile by using high-resolution secondary ion mass spectroscopy (with a sputtering rate of 0.5 Å s^{-1}).

RESULTS AND DISCUSSION

The TMR ratio is strongly dependent on the thickness of the bridging layer in the P-MTJ spin-valves, which was *ex-situ* annealed at the BEOL temperature of 400 °C; that is, the TMR ratio reaches its peak at a specific bridging layer thickness that is measured by current in-plane tunneling at room temperature.[23] Thus, for the p-MTJ spin-valve (stack **A**), a maximum TMR ratio (~97%) was obtained at the bridging and capping layer thickness values of 0.4 and 1.0 nm, respectively, as shown in Supplementary Figure 1. In contrast, for the p-MTJ spin-valve (stack **B**), a maximum TMR ratio (~143%) was achieved at the bridging and capping layer thickness values of 0.24 and 4.0 nm, respectively, as shown in Supplementary Figure 2. Generally, Ta has been widely used as a bridging and capping material for p-MTJ spin-valves.[9,24–27] First, we investigated the dependence of the capping thickness on the TMR ratio for the p-MTJ spin-valves with a top $Co_2Fe_6B_2$ free layer, as shown in Figure 1c. In the p-MTJ spin-valve (stack **A**), the TMR ratio almost decreased linearly from ~97 to 71% when the Ta capping layer thickness increased from ~1.0 to ~2.8 nm, and then it decreased abruptly from ~71 to ~24% when the Ta capping layer thickness increased from ~2.8 to ~3.0 nm. As a result, a maximum TMR ratio (~97%) was obtained at the Ta capping thickness of ~1.0 nm. On the other hand, in the p-MTJ spin-valve (stack **B**), the TMR ratio increased slightly from ~135 to ~143% when the W capping layer thickness increased from ~1.6 to ~4.0 nm, and then it decreased slightly from ~143 to ~133% when the W capping layer thickness increased further. As a result, a maximum TMR ratio (~143%) was obtained at the W capping thickness of ~4.0 nm.

To determine why the TMR ratio of the p-MTJ spin-valve (stack **B**; ~143%) was higher than that of the p-MTJ spin-valve (stack **A**; ~97%), we investigated the static magnetic behavior (the magnetic moment vs magnetic field, that is, the *M–H* curve) of two p-MTJ

spin-valves *ex-situ* annealed at the BEOL temperature of 400 °C, as shown in Figure 2. The p-MTJ spin-valves include four PMA magnetic layers: the $Co_2Fe_6B_2$ free layer (i in Figure 2), the $Co_2Fe_6B_2$ pinned layer (ii in Figure 2), the upper SyAF layer (iii in Figure 2) and the lower SyAF layer (iv in Figure 2). Here, the $Co_2Fe_6B_2$ pinned layer is ferro-coupled with the upper SyAF layer, whereas the upper SyAF layer is anti-ferro-coupled with the lower SyAF layer. In the p-MTJ spin-valve (stack **A**), the magnetic moments of the $Co_2Fe_6B_2$ free layer, the $Co_2Fe_6B_2$ pinned layer ferro-coupled with the upper SyAF layer and the lower SyAF layer were 80 (M_i in the inlet of Figure 2a), 273 (M_{ii+iii} in Figure 2a) and 345 (M_{iv} in Figure 2a) μemu, respectively. In particular, the interface-PMA (i-PMA) characteristics of the p-MTJ spin-valve (the dark *M–H* curve in the inlet of Figure 2a) degraded significantly as a result of Ta diffusion.[28–32] In contrast, in the p-MTJ spin-valve (stack **B**), the magnetic moments of the $Co_2Fe_6B_2$ free layer, the $Co_2Fe_6B_2$ pinned layer ferro-coupled with the upper SyAF layer and the lower SyAF layer were 84 (M_i in the inlet of Figure 2b), 319 (M_{ii+iii} in Figure 2b), and 359 (M_{iv} in Figure 2b) μemu, respectively. In particular, the magnetic moment of the $Co_2Fe_6B_2$ pinned layer ferro-coupled with the upper SyAF layer for the p-MTJ spin-valve (stack **B**; 319 μemu) was higher than that for the p-MTJ spin-valve (stack **A**; 273 μemu). This suggests that the PMA magnetic moment of the $Co_2Fe_6B_2$ pinned layer for the nanoscale-thick W layer was considerably higher than that for the nanoscale-thick Ta layer. In addition, the $Co_2Fe_6B_2$ free layer of the p-MTJ spin-valve (stack **B**) showed excellent i-PMA characteristics (the dark *M–H* curve in the inlet of Figure 2b) and a reasonable coercivity (H_c) to prevent writing errors.[33] The comparison of the *M-H* curves for the p-MTJ spin-valves (stack **A**) and (stack **B**) clearly indicates that the PMA characteristics of both the $Co_2Fe_6B_2$ free and pinned layers for the p-MTJ spin-valve (stack **A**) degraded significantly while those for the p-MTJ spin-valve (stack **B**) were preserved.

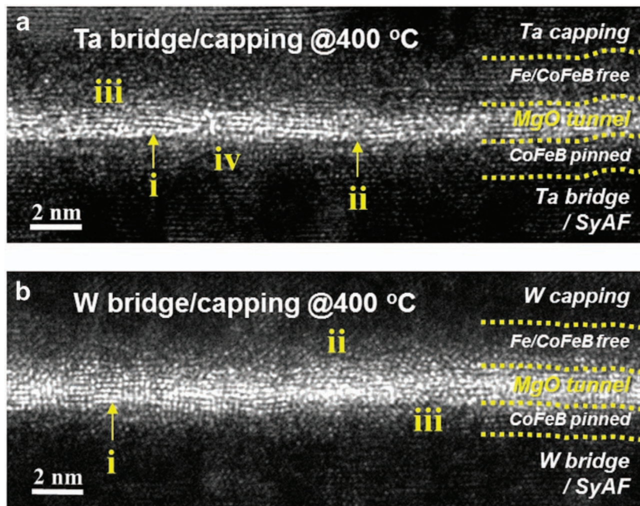

Figure 3 Dependence of fcc crystallinity of the MgO tunneling barrier on the bridging and capping materials for the p-MTJ spin-valve. (**a**) p-MTJ spin-valve with a Ta bridging and capping layer and (**b**) p-MTJ spin-valve with a W bridging and capping layer. Cross-sectional high-resolution TEM images observed at an acceleration voltage of 200 KeV.

Because the PMA characteristics of both the $Co_2Fe_6B_2$ free and pinned layers as well as the fcc crystallinity of the MgO tunneling barrier determine the TMR ratio of the p-MTJ spin-valve, we investigated the difference in the fcc crystallinity of the MgO tunneling barrier for the p-MTJ spin-valves (stack **A**) and (stack **B**) that were *ex-situ* annealed at the BEOL temperature of 400 °C, as shown in Figure 3. In the p-MTJ spin-valve (stack **A**), the MgO tunneling barrier exhibited a combined layer of fcc (100) crystals (i in Figure 3a) and an amorphous layer (ii in Figure 3a), and both the $Co_2Fe_6B_2$ free and pinned layers were revealed to be amorphous layers (iii and iv in Figure 3a), thereby remarkably reducing the *Δ*1 coherent tunneling of the MgO tunneling barrier, which in turn greatly decreased the TMR ratio of the p-MTJ spin-valves.[34] In contrast, in the p-MTJ spin-valve (stack **B**), the MgO tunneling barrier showed an almost complete fcc (100)-crystalized layer (i in Figure 3b). In addition, the $Co_2Fe_6B_2$ free layer appeared as a locally body-centered-cubic-crystalized layer (ii in Figure 3b), whereas the $Co_2Fe_6B_2$ pinned layer appeared as an almost amorphous layer (iii in Figure 3b). These high-resolution TEM results mean that the p-MTJ spin-valve (stack **B**) had significantly better crystallinity than the p-MTJ spin-valve (stack **A**).

To determine why the PMA characteristic and the fcc crystallinity of the MgO tunneling barrier for the p-MTJ spin-valve (stack **B**) appeared to be significantly better than those for the p-MTJ spin-valve (stack **A**), we analyzed the dependence of the atomic compositional depth profiles on the bridging and capping material (that is, Ta or W material), as shown Figure 4. In the p-MTJ spin-valve (stack **A**), a significant amount of Ta atoms diffused into the MgO tunneling barrier from the nanoscale-thick Ta bridging and capping layer, but no W atoms diffused into the MgO tunneling barrier. On the other hand, in the p-MTJ spin-valve (stack **B**), a significant amount of W atoms diffused into the MgO tunneling barrier from the capping and bridging layer but no Ta atoms diffused into the MgO tunneling barrier. In addition, the relative amount of Ta atoms that diffused into the MgO layer (775, arb. unit) and the area of

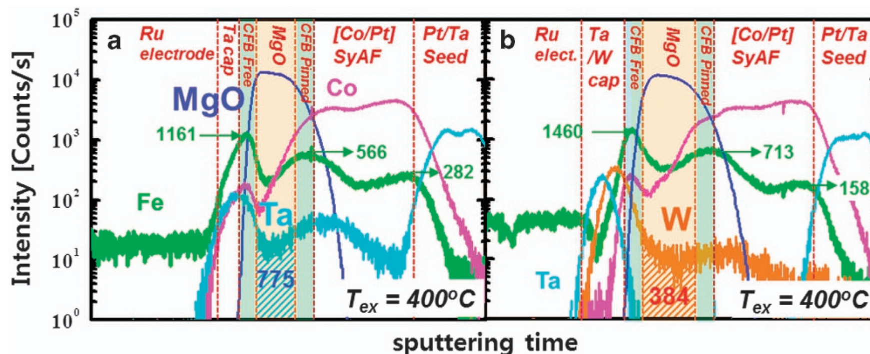

Figure 4 Dependence of atomic compositional depth profile of MgO tunneling barrier on bridging and capping materials for the p-MTJ spin-valves using high-resolution SIMS. (**a**) p-MTJ spin-valve with a Ta bridging and capping layer and (**b**) p-MTJ spin-valve with a W bridging and capping layer.

the Ta atomic concentration in the MgO layer in Figure 4a were approximately two times higher than the relative amount of W atoms that diffused into the MgO barrier (384, arb. unit) and the area of W atomic concentration in the MgO layer, respectively, as shown in Figure 4b. There were two reasons why the degree of degradation of the fcc crystal structure in the MgO tunneling barrier for the Ta bridging and capping layer was higher than that for the W bridging and capping layer. First, the sequence of the atomic diameters is as follows: Ta (2.0 Å), Mg (1.45 Å), and W (1.93 Å). The mismatch between the atomic sizes of Ta and Mg is larger than that between W and Mg, therefore, the lattice strain in the MgO layer induced by the diffusion of Ta atoms would be higher than that induced by the diffusion of W atoms. Thus, the degree of fcc crystallinity degradation in the MgO tunneling barrier for the Ta bridging and capping layer would be higher than that for W bridging and capping layer, when we assume that the same amount of Ta atoms and W atoms diffuse into the MgO layer. Second, since the relative amount of Ta atoms that diffused into the MgO layer was approximately twice as high as that of W atoms in the MgO barrier, the degree of fcc crystallinity degradation of the MgO tunneling barrier for the Ta bridging and capping layer would be higher than that for the W bridging and capping layer. These results agreed with the dependence of the fcc crystallinity of the MgO tunneling barrier on the bridging and capping material; that is, a higher amount of Ta atoms diffusing into the MgO tunneling barrier led to worse fcc crystallinity of the MgO tunneling barrier (compare Figure 3 with Figure 4). In addition, in the p-MTJ spin-valve (stack **A**), the Fe atomic intensities in the $Co_2Fe_6B_2$ free and pinned layers and the SyAF layer were 1161, 566 and 282 counts (arb. unit.), respectively. On the other hand, in the p-MTJ spin-valve (stack **B**), the Fe atomic intensities in the $Co_2Fe_6B_2$ free and pinned layers, and the SyAF layers were 1460, 713 and 158 count (arb. unit), respectively. Thus, the Fe atomic concentrations in the $Co_2Fe_6B_2$ free and pinned layers for the p-MTJ spin-valve (stack **B**) were significantly higher than those for the p-MTJ spin-valve (stack **A**). In addition, the Co atomic concentrations in the $Co_2Fe_6B_2$ free and pinned layers for the p-MTJ spin-valve showed the same trend as the Fe atomic concentrations. These results were probably related to solubility; that is, the solubility of Fe and Co atoms in the W layer was lower than their solubility in the Ta layer, as shown in Supplementary Figure 3. Therefore, the PMA magnetic moments of both $Co_2Fe_6B_2$ free and pinned layers for the p-MTJ spin-valve (stack **B**) were considerably higher than those for the p-MTJ spin-valve (stack **A**). In addition, the diffused Fe atomic concentration from the $Co_2Fe_6B_2$ pinned layer to the SyAF layer for the p-MTJ spin-valve (stack **A**) was significantly higher than that for the p-MTJ spin-valve (stack **A**). Therefore, the PMA property of the $Co_2Fe_6B_2$ pinned layer for the p-MTJ spin-valve (stack **A**) degraded significantly more than that for the p-MTJ spin-valve (stack **A**). In summary, since the PMA characteristics (the magnetic moment) for both the $Co_2Fe_6B_2$ free and pinned layers and the fcc crystallinity of the MgO tunneling barrier for the p-MTJ spin-valve (stack **B**) appeared to be significantly better than those for the p-MTJ spin-valves (stack **A**), the TMR ratio of the p-MTJ spin-valve (stack **B**) (~143%) was considerable higher than that of the p-MTJ spin-valve (stack **A**; ~97%).

CONCLUSION

Recently, P-MTJ spin-valves with top $Co_2Fe_6B_2$ free layers and nanoscale-thick Ta bridging and capping layers have been intensively studied to obtain a higher TMR ratio at a higher *ex-situ* annealing temperature (or BEOL temperature) because this would minimize the diffusion of Pt atoms into the MgO tunneling barrier.[35–37] However, these structures inherently suffer from a significant number of Ta atoms diffusing into the MgO tunneling barrier at an *ex-situ* annealing temperature of 400 °C. Therefore, the fcc crystallinity of the MgO tunneling barrier degrades abruptly, thereby rapidly decreasing the TMR ratio of the P-MTJ spin-valves. Thus, an innovative solution is to fabricate p-MTJ spin-valves with nanoscale-thick W bridging (~0.24 nm) and capping layers (~4.0 nm), which demonstrate no diffusion of Ta atoms into the MgO tunneling barrier and confirm the reduction in diffusing Fe atoms from the $Co_2Fe_6B_2$ free and pinned layers at an *ex-situ* annealing temperature of 400 °C. As a result, the fcc crystallinity degradation of the MgO tunneling barrier is significantly reduced and a high PMA magnetic moment at the $Co_2Fe_6B_2$ free and pinned layers can be achieved, thereby resulting in a TMR ratio of ~143% at an *ex-situ* annealing temperature of 400 °C. The improved fcc crystallinity of the MgO layer for the W capping and bridging layer compared with the Ta capping and bridging layer is likely related to the lower diffusion of metal atoms (W or Ta) and the reduced lattice strain in the MgO layer for the W capping and bridging layer. In addition, the higher Fe and Co atomic concentrations of the $Co_2Fe_6B_2$ free and pinned layers for the W capping and bridging layer are associated with the lower solubilities of Fe and Co atoms in the W layers than in the Ta layers. As a result, the W capping and bridging layer enhanced the TMR ratio compared with the Ta capping and bridging layer.

ACKNOWLEDGEMENTS

This work was supported by a Basic Science Research Program grant from the National Research Foundation of Korea (NRF), which was funded by the Korean government (MSIP; No. 2014R1A2A1A01006474), and the Brain Korea 21 PLUS Program in 2014.

1 Kim, K. N., Chung, U. I., Park, Y. W., Lee, J. Y., Yeo, J. H. & Kim, D. C. Extending the DRAM and FLASH memory technologies to 10 nm and beyond. *Proc. SPIE* **8326**, 832605 (2012).
2 Park, S. K. Technology scaling challenge and future prospects of DRAM and NAND flash memory. *IEEE Int. Memory Workshop* 1–4 (2015).
3 Appuswamy, R., Olma, M. & Ailamaki, A. Scaling the Memory Power Wall With DRAM-Aware Data Management. *Proceedings of the 11th International Workshop on Data Management on New Hardware* 3 (ACM, 2015).
4 Wolf, S. A., Awschalom, D. D., Buhrman, R. A., Daughton, J. M., von Molnár, S., Roukes, M. L., Chtchelkanova, A. Y. & Treger, D. M. Spintronics: a spin-based electronics vision for the future. *Science* **294**, 1488–1495 (2001).
5 Chun, K. C., Zhao, H., Harms, J. D., Kim, T. H., Wang, J. P. & Kim, C. H. A scaling roadmap and performance evaluation of in-plane and perpendicular MTJ based STT-MRAMs for high-density cache memory. *IEEE J. Solid-State Circuits* **48**, 598 (2013).
6 Slonczewski, J. C. Ferromagnetic tunnel junction, magnetoresistive element and magnetic head. US patent 5, 862,022, 19 January 1999.
7 Sun, J. Z. Spin-current interaction with a monodomain magnetic body: a model study. *Phys. Rev. B* **62**, 570 (2000).
8 Ohno, H., Endoh, T., Hanyu, T., Kasai, N. & Ikeda, S. Magnetic tunnel junction for nonvolatile CMOS logic. *IEEE Int. Electron Devices Meeting* 9.4.1-9.4.4 (2010).
9 Ikeda, S., Miura, K., Yamamoto, H., Mizunuma, K., Gan, H. D., Endo, M., Kanai, S., Hayakawa, J., Matsukura, F. & Ohno, H. A perpendicular-anisotropy CoFeB–MgO magnetic tunnel junction. *Nat. Mater.* **9**, 721 (2010).
10 Yakata, S., Kubota, H., Suzuki, Y., Yakushiji, K., Fukushima, A., Yuasa, S. & Ando, K. Influence of perpendicular magnetic anisotropy on spin-transfer switching current in CoFeB/MgO/CoFeB magnetic tunnel junctions. *J. Appl. Phys.* **105**, 07D131 (2009).
11 Lee, D. Y., Shim, T. H. & Park, J. G. Effects of Pt capping layer on perpendicular magnet anisotropy in pseudospin valves of Ta/CoFeB/MgO/CoFeB/Pt magnetic-tunneling junctions. *Appl. Phys. Lett.* **102**, 212409 (2013).
12 Wen, Z. C., Sukegawa, H., Furubayashi, T., Koo, J., Inomata, K., Mitani, S., Hadorn, J. P., Ohkubo, T. & Hono, K. A 4-fold-symmetry hexagonal ruthenium for magnetic heterostructures exhibiting enhanced perpendicular magnetic anisotropy and tunnel magnetoresistance. *Adv. Mater.* **26**, 6483 (2014).
13 Park, J. G., Shim, T. H., Chae, K. S., Lee, D. Y., Takemura, Y., Lee, S. E., Jeon, M. S., Baek, J. U., Park, S. O. & Hong, J. P. Challenging issues for terra-bit-level perpendicular STT-MRAM. *IEEE Int. Electron Devices Meeting* 19.2.1-19.2.4 (2014).
14 Honjo, H., Sato, H., Ikeda, S., Sato, S., Watanebe, T., Miura, S., Nasuno, T., Noguchi, Y., Yasuhira, M., Tanigawa, T., Koike, H., Muraguchi, M., Niwa, M., Ito, K., Ohno, H.

& Endoh, T. 10 nmφ perpendicular-anisotropy CoFeB-MgO magnetic tunnel junction with over 400 °C high thermal tolerance by boron diffusion control. *Symp. VLSI Technol. Dig. Tech. Papers* 160–161 (2015).
15 Lee, S. E., Shim, T. H. & Park, J. G. Co2Fe6B2/MgO-based perpendicular spintransfer-torque magnetic-tunnel-junction spin-valve without [Co/Pt]n lower syntheticantiferro-magnetic layer. *Nanotechnology* **26**, 475705 (2015).
16 Takemura, Y., Lee, D. Y., Lee, S. E., Chae, K. S., Shim, T. H., Lian, G., Kim, M. & Park, J. G. Influence of face-centered-cubic texturing of Co2Fe6B2 pinned layer on tunneling magnetoresistance ratio decrease in Co2Fe6B2/MgO-based p-MTJ spin valves stacked with a [Co/Pd]n-SyAF layer. *Nanotechnology* **26**, 195702 (2015).
17 Kar, G. S., Kim, W., Tahmasebi, T., Swerts, J., Mertens, S., Heylen, N. & Min, T. Co/Ni based p-MTJ stack for sub-20 nm high density stand alone and high performance embedded memory application. *IEEE Int. Electron Devices Meeting* 19.1.1-19.1.4 (2014).
18 Chatterjee, J., Tahmasebi, T., Swerts, J., Kar, G. S. & Boeck, J. D. Impact of seed layer on post-annealing behavior of transport and magnetic properties of Co/Pt multilayer-based bottom-pinned perpendicular magnetic tunnel junctions. *Appl. Phys. Express* **8**, 063002 (2015).
19 Natarajarathinam, A., Zhu, R., Visscher, P. B. & Gupta, S. Perpendicular magnetic tunnel junctions based on thin CoFeB free layer and Co-based multilayer synthetic antiferromagnet pinned layers. *J. Appl. Phys.* **111**, 07C918 (2012).
20 Chang, Y. J., Canizo-Cabrera, A., Garcia-Vazquez, V., Chang, Y. H. & Wu, T. H. Perpendicular magnetic tunnel junctions with synthetic antiferromagnetic pinned layers based on [Co/Pd] multilayers. *J. Appl. Phys.* **113**, 17B909 (2013).
21 Hu, G., Topuria, T., Rice, P. M., Jordan-Sweet, J. & Worledge, D. C. Optimization of Tunneling magnetoresistance in perpendicular magnetic tunnel junctions with Co|Pd reference layers. *IEEE Magn. Lett.* **4**, 3000104 (2013).
22 Peng, S., Wang, M., Yang, H., Zeng, L., Nan, J., Zhou, J., Zhang, Y., Hallal, A., Chshiev, M., Wang, K. L., Zhang, Q. & Zhao, W. Origin of interfacial perpendicular magnetic anisotropy in MgO/CoFe/metallic capping layer structures. *Sci. Rep.* **5**, 18173 (2015).
23 Worledge, D. C. & Trouilloud, P. L. Magnetoresistance measurement of unpatterned magnetic tunnel junction wafers by current-in-plane tunnelling. *Appl. Phys. Lett.* **83**, 84 (2013).
24 Jeon, M. S., Chae, K. S., Lee, D. Y., Takemura, Y., Lee, S. E., Shim, T. H. & Park, J. G. The dependency of tunnel magnetoresistance ratio on nanoscale thicknesses of Co2Fe6B2 free and pinned layers for Co2Fe6B2/MgO-based perpendicular-magnetic-tunnel-junctions. *Nanoscale* **7**, 8142 (2015).
25 Chae, K. S. & Park, J. G. Dependency of tunneling magneto-resistance on Fe insertion-layer thickness in Co2Fe6B2/MgO-based magnetic tunneling junctions. *J. Appl. Phys.* **117**, 153901 (2015).
26 Yakushiji, K., Fukushima, A., Kubota, H., Konoto, M. & Yuasa, S. Ultralow-voltage spin-transfer switching in perpendicularly magnetized magnetic tunnel junctions with synthetic antiferromagnetic reference layer. *Appl. Phys. Express* **6**, 113006 (2013).
27 Sato, H., Yamanouchi, M., Ikeda, S., Fukami, S., Matsukura, F. & Ohno, H. MgO/CoFeB/Ta/CoFeB/MgO recording structure in magnetic tunnel junctions with perpendicular easy axis. *IEEE Trans. Magn.* **49** (7), 4437 (2013).
28 Yang, H. X., Chshiev, M. & Dieny, B. First-principles investigation of the very large perpendicular magnetic anisotropy at Fe|MgO and Co|MgO interfaces. *Phys. Rev. B* **84**, 054401 (2011).
29 Kim, W. J., Jeong, J. H., Kim, Y., Lim, W. C., Kim, J. H., Park, J. H., Shin, H. J., Park, Y. S., Kim, K. S., Park, S. H., Lee, Y. J., Kim, K. W., Kwon, H. J., Park, H. L., Ahn, H. S., Oh, S. C., Lee, J. E., Park, S. O., Choi, S., Kang, H. K. & Chung, C. Extended scalability of perpendicular STT-MRAM towards sub-20 nm MTJ node. *IEEE Int. Electron Devices Meeting* 24.1.1–24.1.4 (2011).
30 Karthik, S. V., Takahashi, Y. K., Ohkubo, T., Hono, K., Ikeda, S. & Ohno, H. Transmission electron microscopy investigation of CoFeB/MgO/CoFeB pseudospin valves annealed at different temperatures. *J. Appl. Phys.* **106**, 023920 (2009).
31 An, G. G., Lee, J. B., Yang, S. M., Kim, J. H., Chung, W. S. & Hong, J. P. Highly stable perpendicular magnetic anisotropies of CoFeB/MgO frames employing W buffer and capping layers. *Acta Mater.* **87**, 259 (2015).
32 Yang, S. M., Lee, J. B., An, G. G., Kim, J. H., Chung, W. S. & Hong, J. P. Ta thickness-dependent perpendicular magnetic anisotropy features in Ta/CoFeB/MgO/W free layer stacks. *Thin Solid Films* **587**, 39–42 (2015).
33 Wang, Z., Zhou, Y., Zhang, J. & Huai, Y. Write error rate in spin transfer torque magnetic random access memory. *SPIN* **02**, 1240001 (2012).
34 Khvalkovskiy, A. V., Apalkov, D., Watts, S., Chepulskii, R., Beach, R. S., Ong, A., Tang, X., Driskill-Smith, A., Butler, W. H., Visscher, P. B., Lottis, D., Chen, E., Nikitin, V. & Krounbi, M. Erratum: basic principles of STT-MRAM cell operation in memory arrays. *J. Phys. D Appl. Phys.* **46**, 074001 (2013).
35 Park, C., Kan, J., Ching, C., Ahn, J., Xue, L., Wang, R., Kontos, A., Liang, S., Bangar, M., Chen, H., Hassan, S., Gottwald, M., Zhu, X., Kang, S. & Pakala, M. Systematic optimization of 1 Gbit perpendicular magnetic tunnel junction arrays for 28 nm embedded STT- MRAM and beyond. *IEEE Int. Electron Devices Meeting* 26.2.1-26.2.4 (2015).
36 Hu, G., Lee, J. H., Nowak, J. J., Sun, J. Z., Harms, J., Annunziata, A., Brown, S., Chen, W., Kim, Y. H., Lauer, G., Liu, L., Marchack, N., Murthy, S., O'Sullivan, E. J., Park, J. H., Reuter, M., Robertazzi, R. P., Trouilloud, P. L., Zhu, Y. & Worledge, D. C. STT-MRAM with double magnetic tunnel junctions. *IEEE Int. Electron Devices Meeting* 26.3.1-26.3.4 (2015).
37 Thomas, L., Jan, G., Le, S., Lee, Y. J., Liu, H., Zhu, J., Serrano-Guisan, S., Tong, R. Y., Pi, K., Shen, D., He, R., Haq, J., Teng, Z., Annapragada, R., Lam, V., Wang, Y. J., Zhong, T., Torng, T. & Wang, P. K. Solving the paradox of the inconsistent size dependence of thermal stability at device and chip-level in perpendicular STT-MRAM. *IEEE Int. Electron Devices Meeting* 26.4.1-26.4.4 (2015).

This work is licensed under a Creative Commons Attribution 4.0 International License. The images or other third party material in this article are included in the article's Creative Commons license, unless indicated otherwise in the credit line; if the material is not included under the Creative Commons license, users will need to obtain permission from the license holder to reproduce the material. To view a copy of this license, visit http://creativecommons.org/licenses/by/4.0/

© The Author(s) 2016

Supplementary Information accompanies the paper on the NPG Asia Materials website (http://www.nature.com/am).